

# Dynamic Phases, Clustering, and Lane Formation for Driven Disk Systems in the Presence of Quenched Disorder

Y. Yang<sup>1,2</sup>, D. McDermott<sup>1,2</sup>, C. J. Olson Reichhardt<sup>1</sup>, and C. Reichhardt<sup>1</sup>

<sup>1</sup>*Theoretical Division, Los Alamos National Laboratory, Los Alamos, New Mexico 87545 USA*

<sup>2</sup>*Department of Physics, Wabash College, Crawfordsville, Indiana 47933, USA*

(Dated: June 21, 2021)

We numerically examine the dynamic phases and pattern formation of two-dimensional monodisperse repulsive disks driven over random quenched disorder. We show that there is a series of distinct dynamic regimes as a function of increasing drive, including a clogged or pile-up phase near depinning, a homogeneous disordered flow state, and a dynamically phase separated regime consisting of high density crystalline regions surrounded by a low density of disordered disks. At the highest drives the disks arrange into one-dimensional moving lanes. The phase separated regime has parallels with phase separation observed in active matter systems, and arises in the disk system due to the combination of nonequilibrium fluctuations and density dependent mobility. We discuss how this system exhibits pronounced differences from previous studies of driven particles moving over random substrates where the particles, such as superconducting vortices or electron crystals, have longer range repulsive interactions, and where dynamical phase separation and strong one-dimensional moving chain effects are not observed. The system we consider could be realized experimentally using sterically interacting colloids driven over random pinning arrays or quasi-two-dimensional granular matter flowing over rough landscapes.

PACS numbers:

## I. INTRODUCTION

A wide range of systems can be effectively modeled as a collection of repulsively interacting particles that are coupled to a substrate that serves as quenched disorder, and these systems typically exhibit a transition from a pinned to a sliding state under an applied external driving force<sup>1</sup>. Examples of such systems include vortices in type-II superconductors<sup>2-4</sup>, driven electron or Wigner crystals<sup>5-7</sup>, skyrmions in chiral magnets<sup>8,9</sup>, charge stabilized colloids<sup>10-12</sup>, and magnetically interacting colloidal systems<sup>13,14</sup>. The depinning transition can either be elastic, where the particles keep their same neighbors, or plastic, where the particles exchange neighbors and break apart<sup>1,3</sup>. In systems with intermediate or long range repulsive particle-particle interactions, the ground state is usually a defect-free triangular lattice. When plastic depinning occurs, pinned and mobile particles coexist, leading to a proliferation of topological defects in the lattice and producing highly disordered particle configurations during plastic flow<sup>1-3</sup>. At higher drives there can be a transition from the plastic flow state to a moving anisotropic crystal<sup>3,15,16</sup> or moving smectic state<sup>17-20</sup>. This transition is associated with an increase in the ordering of the system and produces a distinct change in the structure factor<sup>18-20</sup> and the density of topological defects<sup>18,20</sup> as well as cusps or dips in the transport curves and changes in the fluctuation spectra<sup>20-22</sup>. Depending on the dimensionality and anisotropy of the system, these dynamical transitions can have continuous or first order characteristics<sup>1,3,23</sup>.

In most of the systems where depinning and sliding dynamics have been studied, the repulsive particle-particle interactions are modeled as a smooth potential that is

either long range, as in the case of Coulomb or logarithmic interactions, or screened long range, such as a Bessel function interaction for superconducting vortices or a Yukawa interaction for colloidal systems. There are many systems that have only short range hard disk type particle-particle interactions, such as granular matter or sterically interacting colloids. Hard disk systems can exhibit very different behavior than what is observed in systems with long range repulsion, such as a strong density dependence of the response near a crystallization or jamming transition<sup>24,25</sup>. Two-dimensional (2D) systems with long range repulsive interactions form an ordered solid down to very low densities since the particles are always within interaction range of each other, whereas hard disk systems form a crystalline solid only for the density at which the particles can just touch each other, which corresponds to a packing density or area coverage of  $\phi = 0.9$  for 2D monodisperse nonfrictional disk packings<sup>24</sup>. For densities below the crystallization density, the hard disk system forms a disordered or liquid-like state. It is not clear whether a hard disk assembly driven over random disorder would exhibit the same types of dynamical transitions found for superconducting vortices, Wigner crystals, and colloids, or whether it would simply form a moving disordered state at high drives. Previous studies addressed how pinning and obstacles affect the onset of the jamming transition in bidisperse disk packs<sup>26,27</sup>; however, the driven dynamics for nonzero loading above the jammed states have not been studied. Although it may seem that hard disks driven over quenched disorder would exhibit the same general dynamics, such as dynamical reordering at high drives, as repulsive particle systems with longer range interactions, the question has surprisingly not previously been addressed.

Here we examine an assembly of monodisperse harmonically interacting repulsive disks driven over a random array of pinning sites. We focus on disk densities  $\phi < 0.9$ , below jamming or crystallization. Despite the simplicity of the model, we find that this system exhibits a richer variety of dynamical phases than those observed in studies of longer range repulsive particles driven over random disorder. When the number of pinning sites is smaller than the number of disks, the pinned phase is associated with a pile up or clogging phenomenon in which the system breaks up into clumps or clusters, with unpinned disks prevented from moving by interactions with disks trapped at pinning sites. As the drive is increased beyond depinning, the system enters either a fluctuating uniform disordered state or a phase separated cluster state consisting of a low density gas of disks coexisting with high density clusters. Within the clusters, the disks form a predominantly triangular lattice. The phase separated states generally appear when the driving force is close to the value of the maximum pinning force. For even higher drives, the system can transition into a collection of one-dimensional (1D) moving lanes, and the structure factor exhibits a strong smectic ordering signature. We characterize the different phases and the transitions between them using velocity-force curves, the transverse root mean square displacements, the structure factor, and the density of non-sixfold coordinated particles.

Dynamical phase separation does not normally occur in systems with longer range interactions since the coexistence of a high density and a low density phase would have a prohibitively large energy cost due to the longer range interactions in the dense phase. For the disk system, the energy cost of the particle-particle interactions is zero until the disks come into contact, which occurs only at the highest densities. Similarly, strong 1D laning occurs when the disks can approach each other very closely in the direction of the applied drive without overlapping. It is known that 2D granular systems that undergo inelastic collisions can exhibit cluster instabilities<sup>28,29</sup>; however, in our system there are no frictional contacts between the disks. The density phase separated regime can be understood as a type of active matter clustering effect, where the combination of disk-disk collisions and pinning produce nonequilibrium transverse fluctuations of the disks as well as a density-dependent mobility. Studies of active matter systems with short range particle-particle repulsion and density-dependent mobility show similar clustering behavior<sup>30–33</sup>. At higher drives for the disk system, we find that a uniform moving state forms when the transverse diffusion is lost. Our work suggests that dynamical phase separation and laning effects are general features of driven systems with short range hard disk particle-particle interactions moving over random disorder, which could be realized experimentally by using sterically interacting colloidal assemblies or quasi-2D granular matter flowing over random disorder.

## II. SIMULATION

We consider a 2D system with an area of  $L^2$  with periodic boundary conditions in the  $x$  and  $y$ -direction. The sample contains  $N_d$  harmonically repulsive disks of radius  $R_d$  as well as  $N_p$  pinning sites that are modeled as non-overlapping parabolic potential traps which can exert a maximum pinning force of  $F_p$  on a disk. The disk dynamics are governed by the following overdamped equation of motion:

$$\eta \frac{d\mathbf{R}_i}{dt} = \mathbf{F}_{dd} + \mathbf{F}_p + \mathbf{F}_D. \quad (1)$$

Here  $\eta$  is the damping constant and  $\mathbf{R}_i$  is the location of disk  $i$ . The disk-disk interaction force is  $\mathbf{F}_{dd} = \sum_{i \neq j} k(2R_d - |\mathbf{r}_{ij}|)\Theta(2R_d - |\mathbf{r}_{ij}|)\hat{\mathbf{r}}_{ij}$ , where  $\mathbf{r}_{ij} = \mathbf{R}_i - \mathbf{R}_j$ ,  $\hat{\mathbf{r}}_{ij} = \mathbf{r}_{ij}/|\mathbf{r}_{ij}|$ , and the spring constant  $k = 50$ . The pinning force  $\mathbf{F}_p$  is modeled as arising from randomly placed parabolic attractive wells with a pinning radius of  $r_p = 0.5$ , such that only a single disk can be trapped in a given pinning site at a time.  $F_p$  is the maximum force exerted by the pinning site at the edge of the well. The driving force  $\mathbf{F}_D = F_D \hat{\mathbf{x}}$  is applied along the  $x$  direction, and for each driving force we allow at least  $1 \times 10^6$  simulation time steps to elapse before taking measurements to ensure that the flow has reached a steady state. At each value of  $F_D$  we measure the average disk velocity  $\langle V_x \rangle = N_d^{-1} \sum_{i=1}^{N_d} \mathbf{v}_i \cdot \hat{\mathbf{x}}$ , where  $\mathbf{v}_i$  is the instantaneous velocity of disk  $i$ . The density  $\phi$  of the system is characterized by the packing fraction or the area covered by the disks,  $\phi = N_d \pi R_d^2 / L^2$ , where  $L = 50$  and  $R_d = 0.5$  in dimensionless simulation length units. In the absence of disorder, the disks form a polycrystalline state near  $\phi \approx 0.85$  and a triangular solid at  $\phi \approx 0.9$ . A variation of this model was previously used to study the depinning and jamming of bidisperse disks driven over random pinning; in that work, with a disk radii ratio of 1:1.4, the jamming density in a pin free sample was  $\phi_j \approx 0.845$ <sup>26</sup>.

## III. VARIED DISK DENSITY

We first consider a fixed number of pinning sites  $N_p = 1440$  with  $F_p = 1.0$  as we vary the disk density from  $\phi = 0.05$  to  $\phi = 0.85$ , giving a ratio of pinning sites to disks ranging from  $N_p/N_d = 6.159$  to  $N_p/N_d = 0.37$ . With these parameters, a disk density of  $\phi = 0.31$  corresponds to a ratio of  $N_p/N_d = 1.0$ . Figure 1(a) shows  $\langle V_x \rangle$  versus  $F_D/F_p$  for different values of  $\phi$  and Fig. 1(b) shows the corresponding  $d\langle V_x \rangle/dF_D$  curves. In the inset of Fig. 1(b) we plot the depinning force  $F_c$  vs  $\phi$  indicating that  $F_c$  has a constant value of  $F_c \approx F_p$  at low disk densities  $N_p/N_d > 5.0$ . In this density range, almost every disk can be pinned directly by a pinning site, so collective interactions between the disks do not play an important role in the depinning process; instead, depinning occurs in the single particle limit and the depinning threshold is determined only by the value of  $F_p$ . For  $N_p/N_d < 1.0$ ,

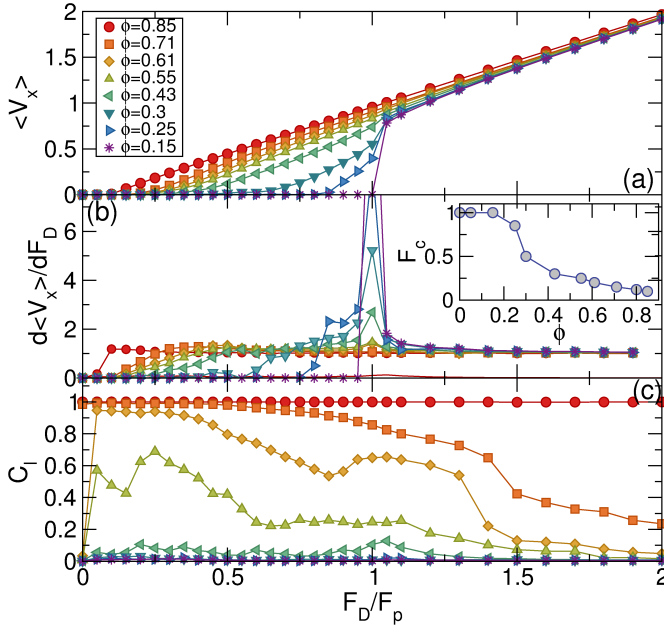


FIG. 1: (a) The average disk velocity  $\langle V_x \rangle$  vs driving force  $F_D/F_p$  for a system of harmonically interacting repulsive disks in a sample with  $F_p = 1.0$  and  $N_p = 1440$  at disk densities of  $\phi = 0.85$  (red circles), 0.71 (orange squares), 0.61 (yellow diamonds), 0.55 (light green up triangles), 0.43 (medium green left triangles), 0.3 (dark green down triangles), 0.25 (blue right triangles), and 0.15 (purple stars). (b) The corresponding  $d\langle V_x \rangle/dF_D$  vs  $F_D/F_p$  curves showing a peak near  $F_D/F_p = 1.0$ . Inset: The depinning threshold  $F_c$  vs  $\phi$ , where  $\phi \approx 0.3$  corresponds to a 1:1 ratio of disks to pinning sites. (c) The corresponding cluster size  $C_l$  vs  $F_D/F_p$ .

some of the disks are not trapped by pinning sites, and these untrapped disks exert a force on the pinned disks which lowers the depinning threshold, as shown in the inset of Fig. 1(a).

In Fig. 1(b), for  $\phi \leq 0.55$  there is a pronounced peak in  $d\langle V_x \rangle/dF_D$  near  $F_D/F_p = 1.0$ . This corresponds to the maximum pinning force from the substrate, so that for  $F_D/F_p > 1.0$  all the disks are moving. For  $N_p/N_d > 0.8$  or  $\phi < 0.4$ , a large fraction of the disks are located at pinning sites and the collision rate is low, so that most of the disks do not become mobile until  $F_D/F_p > 1.0$ , producing the jump in  $\langle V_x \rangle$  at depinning at the lower fillings. For  $N_p/N_d < 1.0$ , there are excess disks that cannot be trapped directly by the pinning sites, and in principle these disks would be mobile for arbitrarily low  $F_D$ ; however, they can still be indirectly pinned or blocked by disks that are located at the pinning sites, creating a local pile up or clogging configuration<sup>26</sup>. Since these interstitial disks exert forces on the disks located at the pinning sites, their presence reduces the depinning threshold by more than a factor of 2. For fillings  $N_p/N_d = 1.0$  to 0.571, corresponding to  $0.3 \leq \phi \leq 0.55$ , some disks remain pinned until  $F_D \geq F_p$ , producing a weak peak in the  $d\langle V_x \rangle/dF_D$  curves at  $F_D/F_p = 1.0$ . When  $\phi$  is

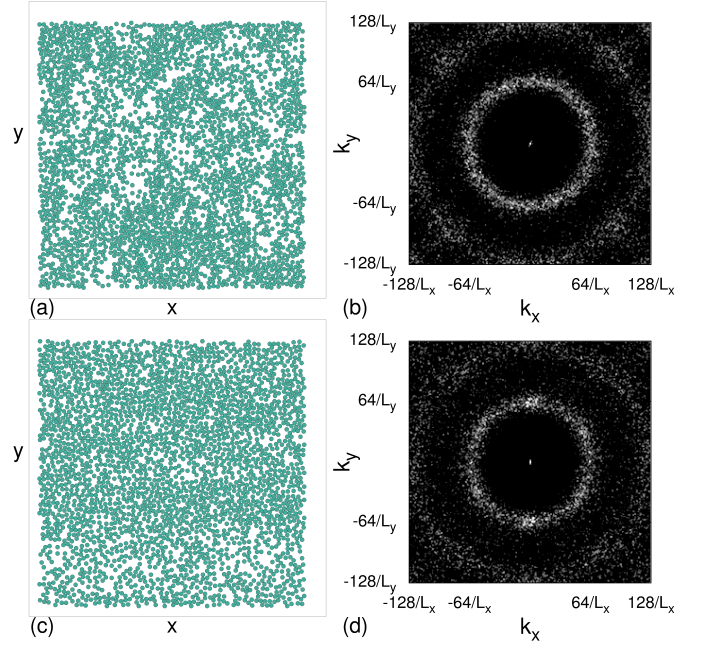


FIG. 2: (a) The disk positions (circles) for the system in Fig. 1 at  $\phi = 0.61$  for  $F_D/F_p = 0.3$ , showing a clustering or pile up effect. (b) The corresponding structure factor  $S(\mathbf{k})$  has a ringlike signature. (c) The driven homogeneous phase in the same system at  $F_D/F_p = 0.7$ . (d) The corresponding  $S(\mathbf{k})$  plot from (c).

large enough, most of the disks are already moving for  $F_D/F_p < 1.0$ , and the peak feature is lost.

In Fig. 1(c) we plot the average value  $C_l$  of the size of the largest cluster normalized by the number of disks in the system as a function of  $F_D/F_p$ . To determine  $C_l$ , we use the cluster counting algorithm of Luding and Herrmann<sup>34</sup>. For  $\phi < 0.43$ ,  $C_l$  is low and the largest clusters contain 10 or fewer disks. For  $\phi \geq 0.43$ , there is an increase in the cluster size at low drives due to a pile up effect in which unpinned disks accumulate behind pinned disks. For  $\phi = 0.85$ , the system forms a large cluster and  $C_l = 1.0$  for all  $F_D$ . At  $\phi = 0.55$ , 0.61, and 0.71, there is a drop off in  $C_l$  for  $F_D/F_p > 1.05$ , 1.33, and 1.4, respectively, indicating a decrease in the cluster size. There is also a local maximum in  $C_l$  near  $F_D/F_p = 1.0$  at  $\phi = 0.61$ .

### A. Intermediate Disk Densities

In Fig. 1(c), for  $\phi = 0.61$  there is an initial increase in  $C_l$  up to  $C_l = 0.95$  at small but finite  $F_D/F_p$  due to the pile up effect. This is followed by a decrease in  $C_l$  to a local minimum near  $F_D/F_p = 0.85$ , and then by another increase to a local maximum in the range  $0.85 < F_D/F_p < 1.4$ , indicating a growth in the size of the largest cluster near  $F_D/F_p = 1.0$ . In Fig. 2(a) we plot the disk configurations for the  $\phi = 0.61$  system at

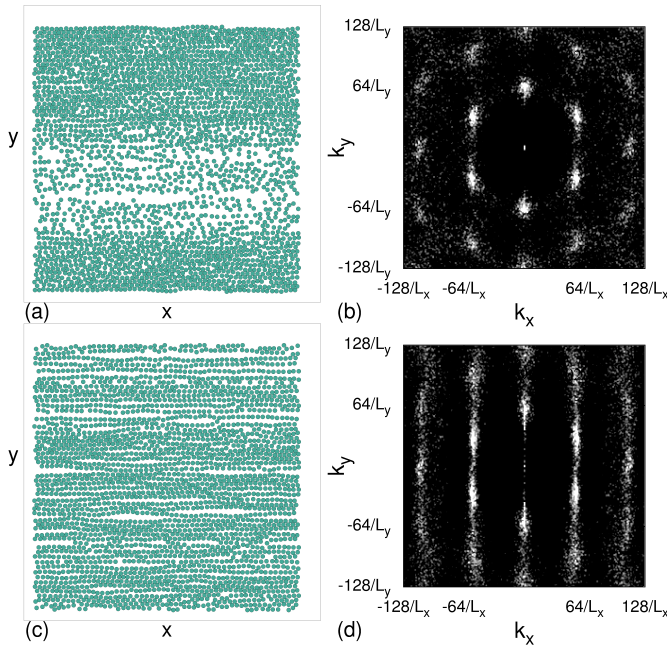


FIG. 3: The disk positions (circles) for the system in Fig. 1 at  $\phi = 0.61$  for  $F_D/F_p = 1.05$ , corresponding to the local maximum in  $C_l$  in Fig. 1(c). Here the system forms a density phase separated state. (b) The corresponding  $S(\mathbf{k})$  plot contains sixfold peaks due to the triangular ordering in the dense phase. (c) The same system at  $F_D/F_p = 2.0$  where a moving chainlike state forms. (d) The corresponding  $S(\mathbf{k})$  shows smectic ordering.

$F_D/F_p = 0.3$  where  $C_l = 0.95$  showing large scale clustering. Similar configurations appear at  $F_D/F_p = 0.3$  for  $0.43 < \phi < 0.85$ . In Fig. 2(b), the corresponding structure factor  $S(\mathbf{k}) = N_d^{-1} |\sum_i \exp(-i\mathbf{k} \cdot \mathbf{r}_i)|^2$  of the disk configuration has a ringlike feature indicative of a disordered system. As the drive is increased beyond the depinning transition, the clusters break apart and the disk density becomes homogeneous, as shown in Fig. 2(c) for  $F_D/F_p = 0.7$ , where a reduction in  $C_l$  has occurred. The corresponding structure factor in Fig. 2(d) still contains a ringlike feature but has excess weight in two peaks along  $k_x = 0$ , indicating the formation of some chainlike structures due to the  $x$ -direction driving.

For  $0.7 < F_D/F_p < 1.4$ , the system forms a density phase separated state, as illustrated in Fig. 3(a) for  $F_D/F_p = 1.05$ . Here there is a high density region with  $\phi \approx 0.85$  in which the disks have triangular ordering coexisting with a low density region where the disks are disordered. The corresponding structure factor in Fig. 3(b) shows six peaks due to the triangular ordering within the dense phase. There is some smearing of the peaks along  $k_y$  due to the tendency of the crystallites in the dense phase to align with the driving direction. For  $F_D/F_p > 1.4$ , where  $C_l$  drops, the disks become more spread out and form 1D moving chains of the type shown in Fig. 3(c) at  $F_D/F_p = 2.0$ . The corresponding  $S(\mathbf{k})$  in

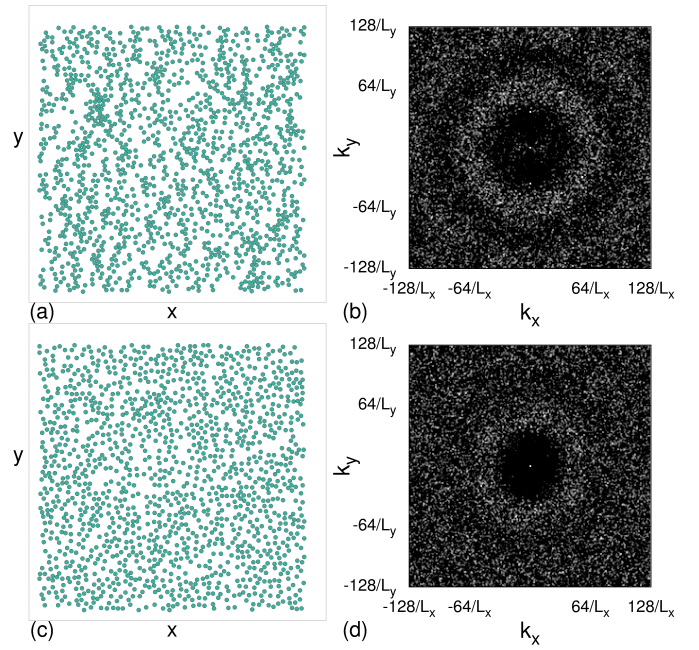


FIG. 4: (a) The disk positions (circles) for the system in Fig. 1 at  $\phi = 0.3$  for  $F_D/F_p = 0.15$ , showing the formation of small clusters. (b) The corresponding  $S(\mathbf{k})$  plot. (c) The same system at  $F_D/F_p = 0.6$  in the moving phase where the disk density becomes homogeneous. (d) The corresponding  $S(\mathbf{k})$  shows a diffuse or liquidlike pattern.

Fig. 3(d) has strong smectic ordering. In general, for  $\phi \geq 0.43$  we find a phase separation in the vicinity of  $F_D/F_p \approx 1$  similar to that shown in Fig. 3(a), where the extent of the dense region grows with increasing  $\phi$  while the low density regions become smaller.

## B. Low Disk Density

For  $\phi < 0.43$ , the clumps that form near depinning are small, as illustrated in Fig. 4(a) at  $\phi = 0.3$  and  $F_D/F_p = 0.15$ . The clumps are anisotropic and show some alignment along the  $y$ -direction, while the corresponding structure factor in Fig. 4(b) has a ringlike signature. At higher drives above depinning when some of the disks are moving, the disk density is more homogeneous, as shown in Fig. 4(c) at  $F_D/F_p = 0.6$ . The corresponding  $S(\mathbf{k})$  plot in Fig. 4(d) has a more diffuse structure. Near  $F_D/F_p = 1.0$ , most of the disks are in motion and form chainlike structures, as illustrated in Fig. 5(a,b) for  $F_D/F_p = 1.05$ . The disk density is not uniform, with some chains closer together and others further apart; however, the denser regions are still too sparse to form sections of triangular lattice of the type that appear at  $\phi = 0.61$  in Fig. 3(a). As  $F_D$  increases for the  $\phi = 0.3$  sample, the moving chains of disks become better defined, as shown in Fig. 5(c) at  $F_D/F_p = 2.0$ . The interchain spacing becomes small enough that the



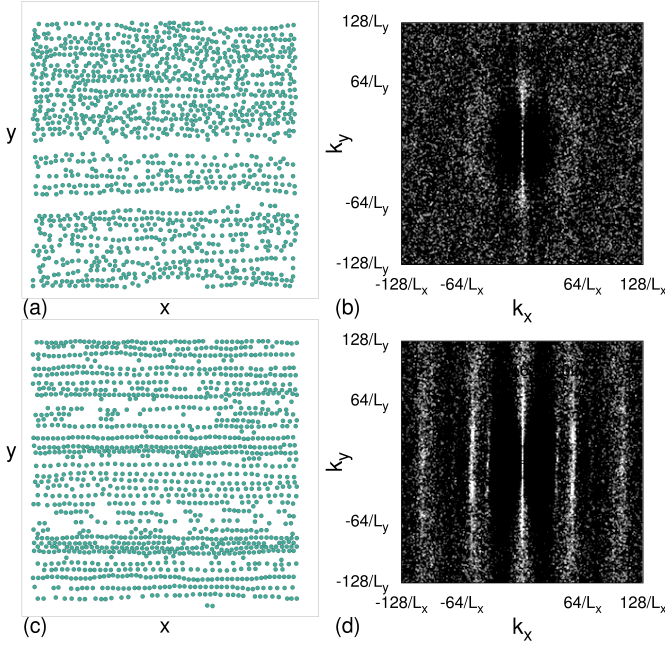


FIG. 5: (a) The disk positions (circles) for the system in Fig. 1 at  $\phi = 0.3$  for  $F_D/F_p = 1.05$ , where the disks form chainlike patterns. (b) The corresponding  $S(\mathbf{k})$  plot. (c) The same system at  $F_D/F_p = 2.0$  in the moving phase where the disks form a series of chains or stripes. (d) The corresponding  $S(\mathbf{k})$  has smectic ordering.

disks in neighboring chains are almost touching, and the corresponding structure factor in Fig. 5(d) shows strong smearing along the  $k_y$  direction.

These results indicate that even though  $\phi$  is below the close-packed density of  $\phi = 0.9$ , different dynamic phases can arise and there can be transitions into states with smectic ordering, similar to the smectic states observed for driven superconducting vortices<sup>7,18–20,22</sup>. In general, the 1D channeling effect illustrated in Fig. 5(c) is much more pronounced in the disk system than in systems with longer range interactions. The moving disks are unstable against the formation of chainlike structures due to a velocity collapse phenomenon. If one moving disk slows down, the disk immediately behind it can run into it and cause it to speed up again, but once the two disks move beyond their steric interaction range, there are no particle-particle interactions to push them further apart, so the disks tend to pile up behind each other in the longitudinal direction. For  $\phi = 0.85$ , the system forms a dense cluster with polycrystalline triangular ordering, and for  $F_D/F_p > 1.0$  the disks form a single triangular domain that is aligned with the driving direction.

### C. Transverse Diffusion and Topological Order

We can characterize the different phases by measuring the particle displacements in the direction transverse

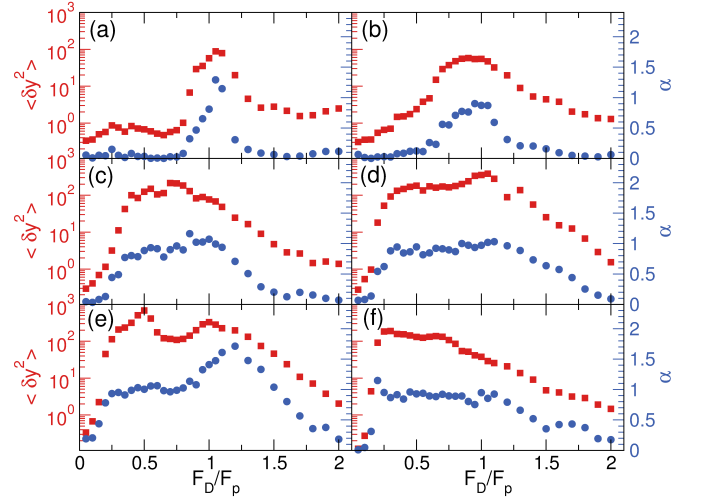


FIG. 6: The transverse displacements  $\langle \delta y^2 \rangle$  obtained after  $4 \times 10^6$  simulation time steps (red squares) and the diffusive exponent  $\alpha$  (blue circles) vs  $F_D/F_p$  for the system in Fig. 1 at  $\phi =$  (a) 0.25, (b) 0.3, (c) 0.43, (d) 0.55, (e) 0.61, and (f) 0.71.

to the applied drive,  $\langle \delta y^2 \rangle = N_d^{-1} \sum_{i=1}^{N_d} (y_i(t) - y_i(t_0))^2$ , for varied  $F_D/F_p$ . In general we find  $\langle \delta y^2 \rangle \propto t^\alpha$  at long times. In the disordered homogeneous density regimes,  $\alpha = 1.0$ , indicative of diffusive behavior, while  $\alpha < 1.0$  just above depinning and in the moving chain state. In Fig. 6 we plot the value of  $\langle \delta y^2 \rangle$  obtained at a fixed time of  $5 \times 10^6$  simulation time steps versus  $F_D/F_p$  along with the corresponding value of  $\alpha$  for the system in Fig. 1 at  $\phi = 0.25, 0.3, 0.43, 0.55, 0.61$ , and  $0.71$ . For  $\phi = 0.25$  and  $\phi = 0.3$  in Fig. 6(a,b), there is a peak in  $\langle \delta y^2 \rangle$  near  $F_D/F_p = 1.0$ , where  $\alpha \approx 1.0$ , indicating diffusive behavior. The maximum amount of transverse diffusion falls at the same value of  $F_D/F_p$  as the peak in  $d\langle V_x \rangle / dF_D$  shown in Fig. 1(b). At low drives where the system forms a clogged state, the transverse diffusion is suppressed. At higher drives where the disks form 1D channels, the diffusion in the direction transverse to the drive is strongly suppressed and  $\alpha \rightarrow 0$ , indicating that the 1D channels are frozen in the transverse direction.

For  $\phi = 0.43, 0.55$ , and  $0.61$  in Fig. 6(c,d,e),  $\langle \delta y^2 \rangle$  has a double peak feature. The first peak corresponds to the onset of the homogeneous moving phase, while the second peak occurs when the system starts to undergo phase separation. For  $\phi = 0.61$ , where the strongest phase separation is observed, there is even a region of drive for which  $\langle \delta y^2 \rangle$  exhibits superdiffusive behavior with  $\alpha > 1.0$ . At longer times the behavior transitions to regular diffusion. For higher drives, both  $\langle \delta y^2 \rangle$  and  $\alpha$  decrease with increasing drive as the system forms a moving chain state. For  $\phi = 0.71$  in Fig. 6(f), the double peak feature begins to disappear. Numerical studies of vortices in type-II superconductors<sup>22,35</sup> show that the vortices exhibit strong transverse diffusion above the depinning transition, while at higher drives where a moving

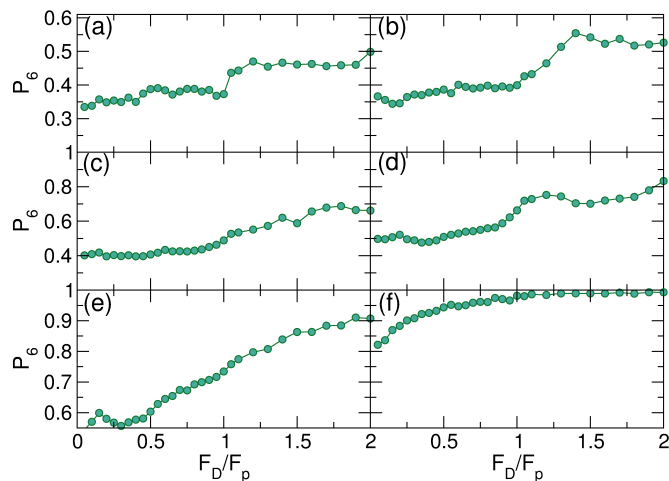


FIG. 7: The fraction  $P_6$  of sixfold coordinated disks vs  $F_D/F_p$  for the system in Fig. 1 for  $\phi =$  (a) 0.25, (b) 0.3, (c) 0.43, (d) 0.61, (e) 0.71, and (f) 0.85. For  $\phi = 0.61$  in panel (d), the local maximum in  $P_6$  near  $F_D = 1.0$  is correlated with the formation of the phase separated state shown in Fig. 3(a).

smectic state appears, the transverse diffusion is strongly suppressed and the system freezes in the transverse direction. The vortex system typically has only a single peak in  $\langle \delta y^2 \rangle$  rather than the double peaks we observe here. The regime of superdiffusive behavior for  $\phi = 0.61$  arises due to collective transverse motion of the disks in the dense phase.

Another measure often used to characterize interacting particles driven over disorder is the fraction  $P_6$  of sixfold coordinated particles. Here  $P_6 = N_d^{-1} \sum_i \delta(z_i - 6)$ , where  $z_i$  is the coordination number of disk  $i$  obtained from a Voronoi tessellation. In the case of superconducting vortices in the absence of pinning, the ground state is a triangular lattice with  $P_6 = 1.0$ , while when strong disorder is present, the pinned state is disordered and contains numerous topological defects so that  $P_6 < 1.0$ . At high drives, where the effect of pinning is reduced, the system can dynamically reorder into a moving triangular lattice with  $P_6 = 1.0$  or into a moving smectic where some topological defects persist that are aligned with the direction of drive, giving  $P_6 \lesssim 1$ <sup>3,4,15,18–20,22</sup>.

In Fig. 7 we plot  $P_6$  versus  $F_D/F_p$  for the system in Fig. 1 at  $\phi = 0.25, 0.3, 0.43, 0.61, 0.71$ , and  $0.85$ . Although there are several similarities to the behavior of  $P_6$  observed for superconducting vortices, there are a number of notable differences. For  $\phi = 0.25$  and  $\phi = 0.3$  in Fig. 7(a,b), there is an increase in  $P_6$  above  $F_D/F_p = 1.0$  which corresponds to the formation of the moving chain state illustrated in Fig. 5(a), followed by a saturation of  $P_6$  at higher drives to  $P_6 = 0.55$ . This is in marked contrast to the behavior observed in the vortex system, where  $P_6$  saturates to a value much closer to  $P_6 = 1.0$  due to the longer range particle-particle repulsion which favors the formation of a triangular vortex lattice down

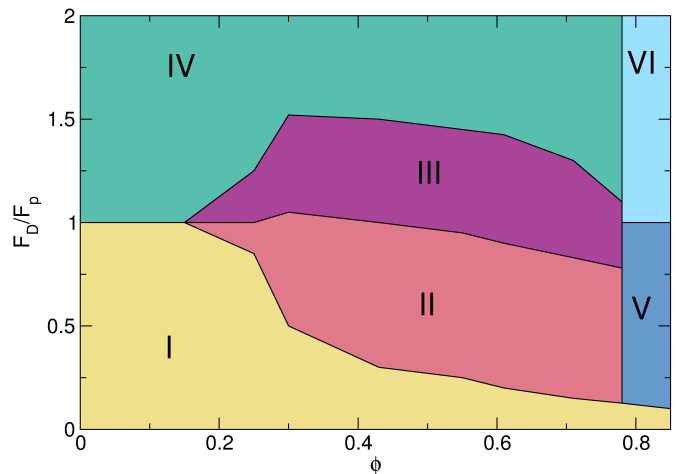


FIG. 8: Schematic phase diagram as a function of  $F_D/F_p$  vs  $\phi$  for the system in Fig. 1. I: Pinned or clogged state. II: Homogeneous plastic flow. III: Density phase separated state. IV: Moving smectic or moving chain state. V: Moving polycrystalline state. VI: Moving crystal state.

to quite low vortex densities. At  $\phi = 0.43$  in Fig. 7(c),  $P_6$  shows a similar trend as in the systems with lower disk densities; however,  $P_6$  saturates to a higher value of  $P_6 = 0.68$ . In Fig. 7(d) at  $\phi = 0.61$ , there is a local maximum in  $P_6$  for  $0.9 < F_D/F_p < 1.4$  that coincides with the density phase separated regime. The disks in the dense phase have mostly triangular ordering, as shown in Fig. 3(a,b). For higher drives of  $F_D/F_p > 1.4$ , where the disks become more spread out,  $P_6$  drops again. At  $\phi = 0.71$  in Fig. 7(e), for low drives  $P_6 \approx 0.55$ , and then  $P_6$  gradually increases with increasing drive up to a value of  $P_6 = 0.9$ , indicating that most of the sample has developed triangular ordering. Finally, for  $\phi = 0.85$  in Fig. 7(f), at the lowest drives the system forms a polycrystalline solid containing a small number of defects, so that the initial value of  $P_6 \approx 0.81$ , while as  $F_D$  increases, the polycrystal anneals into a single domain crystal that is aligned in the direction of drive, with  $P_6 = 0.99$ , indicating almost complete triangular ordering.

For  $0.3 < \phi < 0.85$ , the  $P_6$  curves in Fig. 7 show a small peak near  $F_D/F_p = 0.2$  due to the pile up or clustering effect. Within the clusters the local density  $\phi_{loc}$  is  $\phi_{loc} \approx 0.85$ , producing increased sixfold ordering and a corresponding increase in  $P_6$ . Once the drive is large enough to break apart these clusters, there is a drop in  $P_6$  as the system enters the homogeneous moving phase.

From the features in the velocity-force curves,  $P_6$ ,  $\langle \delta y^2 \rangle$ , and the disk configurations, we can construct a schematic phase diagram of the evolution of the different phases, as shown in Fig. 8. Phase I corresponds to the pinned or clogged state, phase II is homogeneous disordered plastic flow, phase III is the density phase separated state, phase IV is the moving smectic or moving chain state, phase V is the moving polycrystalline state,

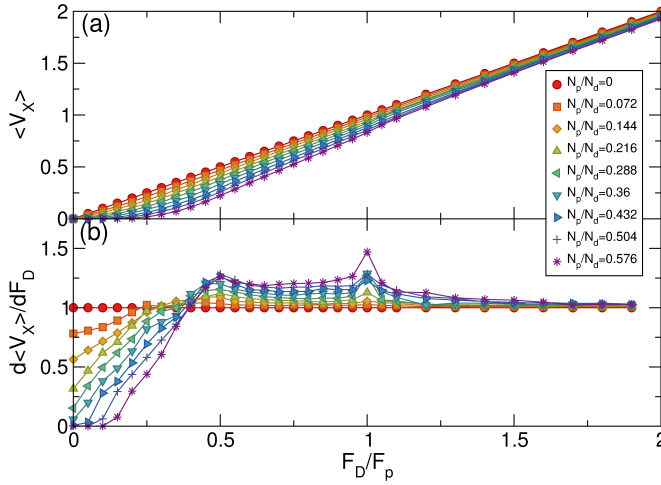


FIG. 9: (a)  $\langle V_x \rangle$  vs  $F_D/F_p$  at  $\phi = 0.55$  and  $F_p = 1.0$  for  $N_p/N_d = 0.0, 0.072, 0.144, 0.216, 0.288, 0.36, 0.432, 0.504$ , and  $0.576$ , from top to bottom. (b) The corresponding  $d\langle V_x \rangle/dF_D$  vs  $F_D/F_p$  curves showing peaks near  $F_D/F_p = 0.5$  and  $F_D/F_p = 1.0$ .

and phase VI is the moving single domain crystal state. At low  $\phi$  where few disk-disk collisions occur, the system passes directly from a pinned state for  $F_D/F_p < 1.0$  to a moving state that is similar to the moving chain state illustrated in Fig. 5. As  $\phi$  increases, the depinning threshold drops due to collisions between unpinned and pinned disks, and above depinning the system enters a homogeneous plastic flow state similar to that shown in Fig. 2(c,d). At higher drives, the density phase separated state illustrated in Fig. 3(a) forms, followed by a transition to the moving chain state shown in Fig. 3(d). For  $\phi > 0.77$ , the disks depin into a moving polycrystalline state which transitions to a single moving crystal at high drives. We expect that for  $\phi \geq 0.9$ , the system would form a crystalline pinned or jammed state that would depin elastically into a moving single crystal state.

#### IV. VARIED PINNING DENSITY

We next consider the case of a fixed disk density of  $\phi = 0.55$ , where  $N_d = 2500$ , and vary the number of pinning sites to give a ratio of  $N_p/N_d$  ranging from  $N_p/N_d = 0$  to  $N_p/N_d = 0.576$ . In Fig. 9(a,b) we show  $\langle V_x \rangle$  and  $d\langle V_x \rangle/dF_D$  versus  $F_D/F_p$  for a sample with  $F_p = 1.0$ . There is one peak in  $d\langle V_x \rangle/dF_D$  near  $F_D/F_p = 1.0$ , the drive above which all of the disks are moving, and a second peak near  $F_D/F_p = 0.5$ , the drive at which the clogged state breaks apart. We observe a similar set of phases as described above, but find that the density phase separated state is more prominent at lower pinning density, as shown in the plots of  $C_l$  versus  $F_D/F_p$  in Fig. 10 for  $N_p/N_d = 0.072, 0.216, 0.288$ , and  $0.432$ . In particular,  $N_p/N_d = 0.216$  in Fig. 10(b) and  $N_p/N_d = 0.288$  in Fig. 10(c) exhibit strong peak features

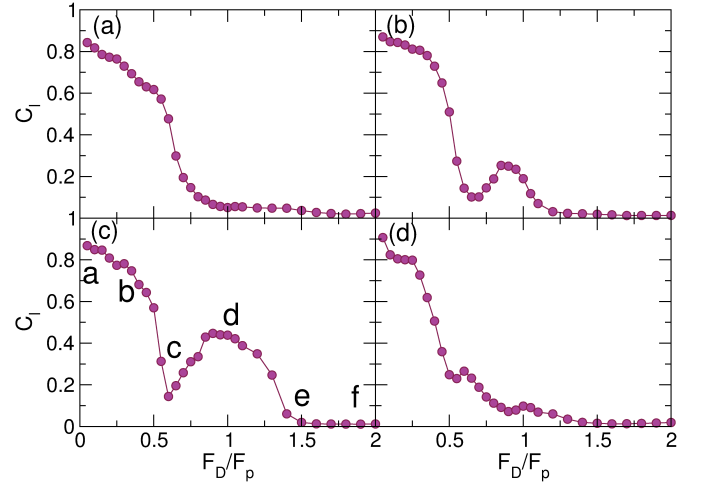


FIG. 10: Cluster size  $C_l$  vs  $F_D/F_p$  for the system in Fig. 9 at  $N_p/N_d =$  (a) 0.072, (b) 0.216, (c) 0.288, and (d) 0.432. The local peaks in (b) and (c) correspond to the formation of a density phase separated state. In panel (c) the lettering indicates the  $F_D/F_p$  values represented in the real space images in Fig. 11.

associated with the density phase separated state.

To show more clearly the evolution of the cluster state, in Fig. 11 we illustrate the disk positions for the system at  $N_p/N_d = 0.288$  for increasing  $F_D$ . The letters a through f in Fig. 10(c) indicate the values of  $F_D/F_p$  that match the images. In Fig. 11(a) at  $F_D/F_p = 0.05$ , where  $C_l = 0.85$ , the system forms a clogged state. Within the cluster regions, which are colored red, the disk density is close to  $\phi = 0.85$ , and these clusters are separated by low density regions of disks. As the drive increases, the large cluster becomes more spread out, as shown in Fig. 11(b) for  $F_D/F_p = 0.3$ , where  $C_l$  drops to  $C_l = 0.78$ . At  $F_D/F_p = 0.6$  in Fig. 11(c), which corresponds to a local minimum in  $C_l$  in Fig. 10(c), the disks are completely spread out and form a homogeneous disordered phase. In Fig. 11(d) at  $F_D/F_p = 1.05$ , which corresponds to a local maximum in  $C_l$  in Fig. 10(c), a density phase separated state appears. Disks that are in a cluster containing at least three disks are colored red in order to more clearly highlight the dense region, within which the disks have developed triangular ordering. As the drive is further increased, the disks spread apart in the direction transverse to the drive to form the moving chain state illustrated in Fig. 11(e,f) at  $F_D/F_p = 1.5$  and  $F_D/F_p = 2.0$ , respectively, which also coincides with a reduction of  $C_l$  in Fig. 10(c). For  $N_p/N_d = 0.55$  and above, the density phase separated state becomes less well defined, as indicated in Fig. 10(d) at  $N_p/N_d = 0.432$ .

In Fig. 10(a) at  $N_p/N_d = 0.072$ , although  $C_l$  does not show a peak near  $F_D/F_p = 1.0$ , there is still a pronounced density phase separated state; however, this phase has shifted to lower  $F_D/F_p$ . Since the low density clogged state transitions directly into the flowing density phase separated state, there is no dip in  $C_l$ . The



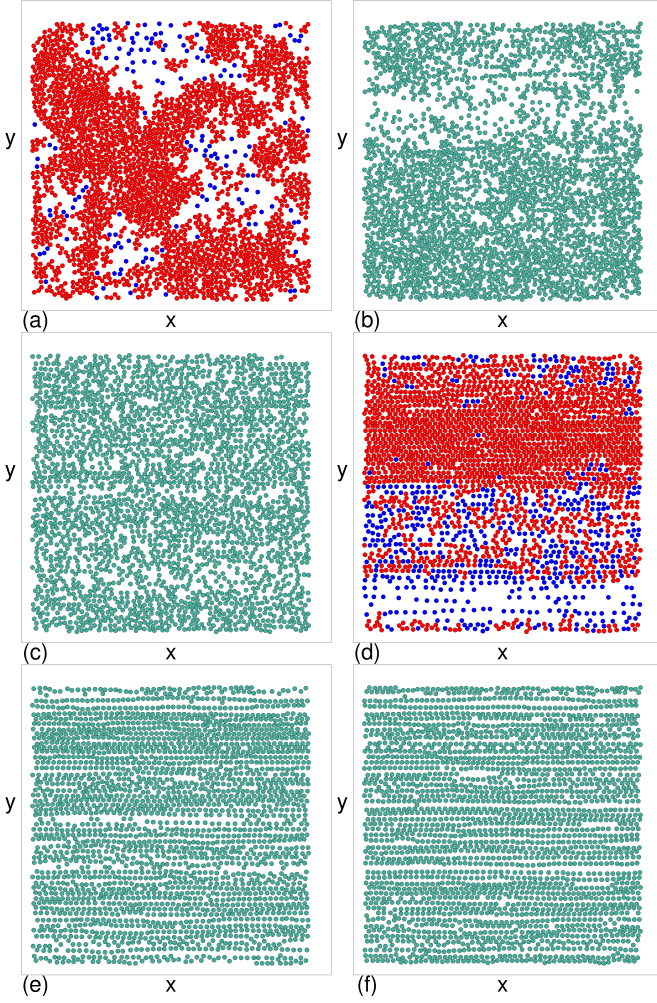


FIG. 11: The disk positions for the system in Figs. 9 and 10 at  $N_p/N_d = 0.288$  for drive values marked with letters in Fig. 10(c). In panels (a) and (d), red disks are part of clusters containing three or more disks, while blue disks are isolated or in a cluster containing only two disks. (a) The pinned cluster state at  $F_D/F_p = 0.05$ . (b) At  $F_D/F_p = 0.3$  the moving disks form more spread out clusters. (c) At  $F_D/F_p = 0.6$ , corresponding to the local minimum of  $C_l$  in Fig. 10(c), a homogeneous disordered state forms. (d) At  $F_D/F_p = 1.05$ , corresponding to the peak in  $C_l$  in Fig. 10(c), a density phase separated state forms. At (e)  $F_D/F_p = 1.5$  and (f)  $F_D/F_p = 2.0$ , the disks are in a moving chain state.

density phase separated state breaks apart at lower values of  $F_D/F_p$  compared to samples with higher values of  $N_p/N_d$ . In Fig. 12(a) we show the disk configurations at  $N_p/N_d = 0.072$  and  $F_D/F_p = 0.3$  where a density phase separated state appears, while in Fig. 12(b) we illustrate the moving chain phase that forms at  $F_D/F_p = 1.5$  in the same system. From the images we can construct a schematic phase diagram for the  $\phi = 0.55$  sample as a function of  $F_D/F_p$  versus  $N_p/N_d$ , as shown in Fig. 13(a), which highlights the extents of regions I through IV. Here, the widths of regions I and II grow with increasing

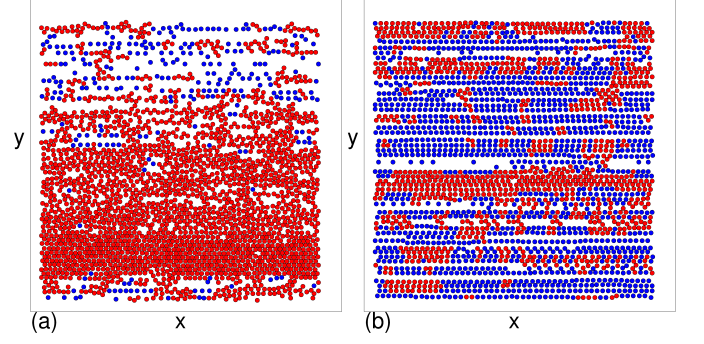


FIG. 12: The disk positions for a system with  $\phi = 0.55$  at  $N_p/N_d = 0.072$ , where there is no peak in  $C_l$  in Fig. 10(a). Red disks are part of clusters containing three or more disks, while blue disks are isolated or in a cluster containing only two disks. (a) A density phase separated state at  $F_D/F_p = 0.3$ . (b) A moving chain state forms at higher drives, shown here at  $F_D/F_p = 1.5$ .

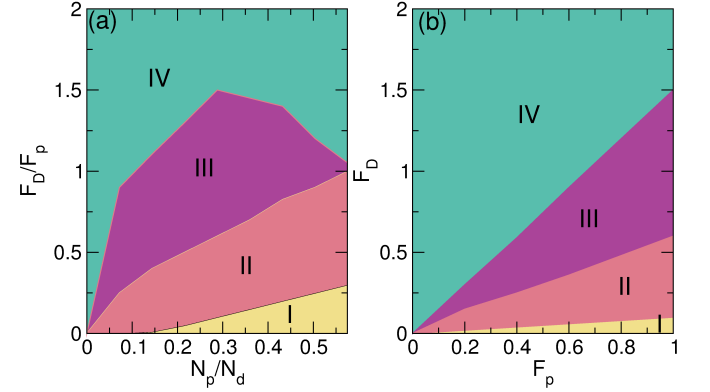


FIG. 13: (a) Schematic phase diagram as a function of  $F_D/F_p$  vs  $N_p/N_d$  for the system in Fig. 9 at fixed  $\phi = 0.55$ . I: Pinned or clogged state. II: Homogeneous plastic flow. III: Density phase separated state. IV: Moving smectic or moving chain state. (b) Phase diagram for the same system at  $\phi = 0.55$  and  $N_p/N_d = 0.288$  as a function of  $F_D$  vs  $F_p$ .

$N_p/N_d$ , while region III reaches its largest extent near  $N_p/N_d = 0.3$ . We note that for  $N_p/N_d = 0$ , the system forms a moving disordered state for all  $F_D > 0$ .

We have considered varying  $F_p$  while holding  $\phi$  and  $N_p/N_d$  fixed, and find that the same general phases appear. The onset of the phases shifts linearly to higher values of  $F_D$  with increasing  $F_p$ , as shown in the phase diagram of  $F_D$  versus  $F_p$  in Fig. 13(b). In Fig. 14(a) we plot  $C_l$  versus  $F_D$  in a sample with  $\phi = 0.55$  and  $N_p/N_d = 0.288$  for  $F_p = 0.0, 0.2, 0.4, 0.6$ , and  $1.0$ . The width of the peak in  $C_l$  associated with density phase separation shifts to higher values of  $F_D$  with increasing  $F_p$ .

For depinning in systems with longer range interactions, such as superconducting vortices, colloidal particles, and electron crystals, scaling near the depinning threshold has been observed in the velocity-force curves,



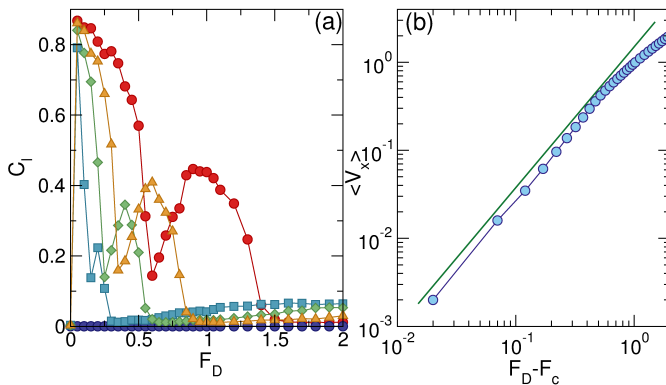


FIG. 14: (a) The cluster size  $C_l$  vs  $F_D$  for samples with  $\phi = 0.55$  and  $N_p/N_d = 0.288$  at  $F_p = 0.0$  (blue circles), 0.2 (blue squares), 0.4 (green diamonds), 0.6 (orange triangles), and 1.0 (red circles). (b)  $\langle V_x \rangle$  vs  $F_D - F_c$  for the velocity-force curve obtained at  $\phi = 0.55$  and  $N_p/N_d = 0.576$ . The solid line is a power law fit with an exponent of  $\beta = 1.6$ .

which have the form  $V \propto (F_D - F_c)^{-\beta}$ . In plastic depinning, where particles exchange neighbors as they move,  $\beta > 1.0$ , while for elastic depinning, in which the particles maintain the same neighbors as they move,  $\beta < 1.0$ <sup>1</sup>. In systems with long range Coulomb interactions<sup>6</sup> and screened Coulomb interactions<sup>10,36</sup>, plastic depinning is associated with exponents of  $\beta \approx 1.65$  and  $\beta \approx 2.0$ , respectively. More recently, simulations of depinning of superconducting vortices with a Bessel function vortex-vortex interaction give  $\beta = 1.3$ <sup>37</sup>. Thus, it is interesting to ask whether similar scaling of the velocity-force curves occurs in the disk system. In Fig. 14(b) we plot  $\langle V_x \rangle$  versus  $F_D - F_c$  on a log-log scale for a sample with  $\phi = 0.55$  at  $N_p/N_d = 0.576$ . The solid line indicates a scaling fit with  $\beta = 1.6$ . At higher drives, well above depinning, the slope of the velocity-force curve becomes linear, as expected since the effectiveness of the pinning is lost in this regime. In general, we find that for  $N_p/N_d > 0.288$ , the velocity-force curves can be fit to a power law with  $1.4 < \beta < 1.7$ . For  $N_p/N_d < 0.288$ , the depinning threshold  $F_c = 0$  since there are few enough pinning sites that some disks can pass completely through the system without being trapped directly by pinning or indirectly by becoming lodged behind pinned disks. This result indicates that scaling near the depinning threshold for plastic flow is robust in systems with short range repulsion as well as in those with longer range repulsion.

## V. DISCUSSION

The dynamic density phase separation we find has not been observed in studies of superconducting vortices or colloids driven over random disorder. There have been cases where a phase separation into high density regions as well as stripe ordering occurs for particles driven over random disorder when the pairwise interactions be-

tween particles include both a repulsive and an attractive term<sup>38,39</sup>; however, in the disk system we consider here, the disk-disk interaction is purely repulsive. The phase separation we observe can be viewed as an example of active matter clustering of the type found in simulations of hard disks undergoing active Brownian motion or run-and-tumble type dynamics. In the active matter systems, when the activity is high enough, the particles phase separate into a dense solidlike region and a low density fluid<sup>30–33</sup> due to a combination of the nonequilibrium nature of the fluctuations and the fact that the mobility of the particles is dependent on the local particle density<sup>31</sup>. In the driven disk system, velocity fluctuations transverse to the driving direction are generally largest when there is a coexistence of disks being pinned or slowed down by the pinning along with faster moving unpinned disks. When the disks collide with each other, they generate velocity fluctuations that have a ballistic component in the transverse direction, similar to the motion of active particles. This also produces time intervals in the transverse diffusion that exhibit superdiffusive behavior similar to that found in active matter systems<sup>33</sup>. Additionally, the disks have a reduced mobility when the disk density increases. When the drive is large enough, both the speed differential of the disks and the velocity fluctuations transverse to the drive are lost, and since these effects are necessary to produce the clustering and the density phase separation, the clustering and density phase separation also disappear. The same effects could arise in systems with longer range interactions; however, the large energy cost of high density regions would suppress the density phase separation we observe for the short range repulsive disks. Experimentally, the dynamic phase separation could be observed using colloids that have only steric interactions moving over random substrate. Experiments with quasi-2D granular systems could include grains flowing over a rough landscape under the influence of gravity or shaking. In our work we focus on the case of monodisperse disks, so that the system forms triangular ordering in the dense phase. We expect that many of the general results should remain robust in nonmonodisperse systems; however, the phases may shift to lower densities since it is known that bidisperse disk systems exhibit jamming at a lower density than monodisperse disks<sup>25</sup>. In addition, the bidisperse disks would have an amorphous structure in the dense phase separated regions. There could be additional behavior that arises in nonmonodisperse systems since the flow could induce a phase separation of the different species of disks, as well as a density phase separation.

## VI. SUMMARY

We have numerically examined the dynamical phases for monodisperse repulsive disks driven over random disorder. Despite the simplicity of this system, we observe a rich variety of distinct dynamics, many of which have

significant differences from the dynamic phases observed for other systems of collectively interacting particles with longer range repulsion, such as vortices in type-II superconductors and colloids with Yukawa interactions. The phases we find include a heterogeneous clogged state where the disks form local immobile clumps, a homogeneous disordered plastic flow state, a moving density phase separated state where the system forms a dense region with mostly triangular ordering coexisting with a low density disordered phase, and a stripe or chain-like state at higher drives. The density phase separation occurs due to the density dependent mobility of the disks and the short range nature of their interaction with each other, which permits the disks to pack closely together with little overlap energy. In contrast, in vortices, Coulomb systems, and charged colloids, the longer range repulsion would prevent density phase separated states from forming since more homogeneous states would have a much lower particle-particle interaction energy. From

the features in the transverse diffusion, structure factor, and velocity-force curves, we map the evolution of the different phases as a function of disk density, pinning site density, and pinning force. Our results suggest that the dynamic density phase separation and the chainlike state should be general features in systems with short range steric interactions driven over random disorder. These effects could be observed experimentally using sterically interacting colloids or granular matter flowing over random disorder.

### Acknowledgments

This work was carried out under the auspices of the NNSA of the U.S. DoE at LANL under Contract No. DE-AC52-06NA25396.

- 
- <sup>1</sup> C. Reichhardt and C.J. Olson Reichhardt, Depinning and nonequilibrium dynamic phases of particle assemblies driven over random and ordered substrates: a review, arXiv:1602.03798 (unpublished).
  - <sup>2</sup> H.J. Jensen, A. Brass, Y. Brechet, and A.J. Berlinsky, Current-voltage characteristics in a two-dimensional model for flux flow in type-II superconductors, *Phys. Rev. B* **38**, 9235 (1988).
  - <sup>3</sup> S. Bhattacharya and M. J. Higgins, Dynamics of a disordered flux line lattice, *Phys. Rev. Lett.* **70**, 2617 (1993).
  - <sup>4</sup> M. C. Faleski, M. C. Marchetti, and A. A. Middleton, Vortex dynamics and defects in simulated flux flow, *Phys. Rev. B* **54**, 12427 (1996).
  - <sup>5</sup> M.-C. Cha and H. A. Fertig, Topological defects, orientational order, and depinning of the electron solid in a random potential, *Phys. Rev. B* **50**, 14368 (1994).
  - <sup>6</sup> C. Reichhardt, C. J. Olson, N. Grønbech-Jensen, and F. Nori, Moving Wigner glasses and smectics: Dynamics of disordered Wigner crystals, *Phys. Rev. Lett.* **86**, 4354 (2001).
  - <sup>7</sup> G. Csáthy, D. Tsui, L. Pfeiffer, and K. West, Stability and negative differential resistance of the Wigner solid, *Phys. Rev. Lett.* **98**, 066805 (2007).
  - <sup>8</sup> T. Schulz, R. Ritz, A. Bauer, M. Halder, M. Wagner, C. Franz, C. Pfeiderer, K. Everschor, M. Garst, and A. Rosch, Emergent electrodynamics of skyrmions in a chiral magnet, *Nature Phys.* **8**, 301 (2012).
  - <sup>9</sup> C. Reichhardt, D. Ray, and C.J. Olson Reichhardt, Collective transport properties of driven skyrmions with random disorder, *Phys. Rev. Lett.* **114**, 217202 (2015).
  - <sup>10</sup> C. Reichhardt and C. J. Olson, Colloidal dynamics on disordered substrates, *Phys. Rev. Lett.* **89**, 078301 (2002).
  - <sup>11</sup> A. Pertsinidis and X.S. Ling, Statics and dynamics of 2D colloidal crystals in a random pinning potential, *Phys. Rev. Lett.* **100**, 028303 (2008).
  - <sup>12</sup> S. Deutschländer, T. Horn, H. Löwen, G. Maret, and P. Keim, Two-dimensional melting under quenched disorder, *Phys. Rev. Lett.* **111**, 098301 (2013).
  - <sup>13</sup> Y.G. Cao, Q.X. Li, G.Y. Fu, J. Liu, H.Z. Guo, X. Hu, and X.J. Li, Depinning dynamics of two-dimensional magnetized colloids on a random substrate, *J. Phys.: Condens. Matter* **22**, 155101 (2010).
  - <sup>14</sup> P. Tierno, Depinning and collective dynamics of magnetically driven colloidal monolayers, *Phys. Rev. Lett.* **109**, 198304 (2012).
  - <sup>15</sup> A. E. Koshelev and V. M. Vinokur, Dynamic melting of the vortex lattice, *Phys. Rev. Lett.* **73**, 3580 (1994).
  - <sup>16</sup> P. Le Doussal and T. Giamarchi, Moving glass theory of driven lattices with disorder, *Phys. Rev. B* **57**, 11356 (1998).
  - <sup>17</sup> L. Balents, M.C. Marchetti, and L. Radzihovsky, Nonequilibrium steady states of driven periodic media, *Phys. Rev. B* **57**, 7705 (1998).
  - <sup>18</sup> K. Moon, R.T. Scalettar, and G.T. Zimányi, Dynamical phases of driven vortex systems, *Phys. Rev. Lett.* **77**, 2778 (1996).
  - <sup>19</sup> F. Pardo, F. de la Cruz, P.L. Gammel, E. Bucher, and D.J. Bishop, Observation of smectic and moving-Bragg-glass phases in flowing vortex lattices, *Nature (London)* **396**, 348 (1998).
  - <sup>20</sup> C.J. Olson, C. Reichhardt, and F. Nori, Nonequilibrium dynamic phase diagram for vortex lattices, *Phys. Rev. Lett.* **81**, 3757 (1998).
  - <sup>21</sup> A.C. Marley, M.J. Higgins, and S. Bhattacharya, Flux flow noise and dynamical transitions in a flux line lattice, *Phys. Rev. Lett.* **74**, 3029 (1995).
  - <sup>22</sup> A. Kolton, D. Domínguez, and N. Grønbech-Jensen, Hall noise and transverse freezing in driven vortex lattices, *Phys. Rev. Lett.* **83**, 3061 (1999).
  - <sup>23</sup> M.C. Marchetti, A.A. Middleton, K. Saunders, and J.M. Schwarz, Driven depinning of strongly disordered media and anisotropic mean-field limits, *Phys. Rev. Lett.* **91**, 107002 (2003).
  - <sup>24</sup> C. Reichhardt and C. J. Olson Reichhardt, Aspects of jamming in two-dimensional athermal frictionless systems, *Soft Matter* **10**, 2932 (2014).
  - <sup>25</sup> C.S. O'Hern, L.E. Silbert, A.J. Liu, and S. R. Nagel, Jamming at zero temperature and zero applied stress: The

- epitome of disorder, *Phys. Rev. E* **68**, 011306 (2003).
- <sup>26</sup> C.J. Olson Reichhardt, E. Groopman, Z. Nussinov, and C. Reichhardt, Jamming in systems with quenched disorder, *Phys. Rev. E* **86**, 061301 (2012).
  - <sup>27</sup> A.L. Graves, S. Nashed, E. Padgett, C.P. Goodrich, A.J. Liu, and J.P. Sethna, Pinning susceptibility: The effect of dilute, quenched disorder on jamming, *Phys. Rev. Lett.* **116**, 235501 (2016).
  - <sup>28</sup> A. Kudrolli, M. Wolpert, and J. P. Gollub Cluster formation due to collisions in granular material, *Phys. Rev. Lett.* **78**, 1383 (1997).
  - <sup>29</sup> I. Aranson and L. Tsimring, Patterns and collective behavior in granular media: Theoretical concepts, *Rev. Mod. Phys.* **78**, 641 (2006).
  - <sup>30</sup> J. Tailleur and M.E. Cates, Statistical mechanics of interacting run-and-tumble bacteria, *Phys. Rev. Lett.* **100**, 218103 (2008).
  - <sup>31</sup> M.E. Cates and J. Tailleur, When are active Brownian particles and run-and-tumble particles equivalent? Consequences for motility-induced phase separation, *Europhys. Lett.* **101**, 20010 (2013).
  - <sup>32</sup> C. Reichhardt and C.J. Olson Reichhardt, Active microrheology in active matter systems: Mobility, intermittency, and avalanches, *Phys. Rev. E* **91**, 032313 (2015).
  - <sup>33</sup> C. Bechinger, R. Di Leonardo, H. Löwen, C. Reichhardt, G. Volpe, and G. Volpe, Active Brownian particles in complex and crowded environments, *Rev. Mod. Phys.*, in press (2016).
  - <sup>34</sup> S. Luding and H.J. Herrmann, Cluster-growth in freely cooling granular media, *Chaos* **9**, 673 (1999).
  - <sup>35</sup> C. J. Olson, C. Reichhardt, and F. Nori, Fractal networks, braiding channels, and voltage noise in intermittently flowing rivers of quantized magnetic flux, *Phys. Rev. Lett.* **80**, 2197 (1998).
  - <sup>36</sup> C. Reichhardt and C.J. Olson Reichhardt, Charge transport transitions and scaling in disordered arrays of metallic dots, *Phys. Rev. Lett.* **90**, 046802 (2003).
  - <sup>37</sup> Y. Fily, E. Olive, N. Di Scala, and J. C. Soret, Critical behavior of plastic depinning of vortex lattices in two dimensions: Molecular dynamics simulations, *Phys. Rev. B* **82**, 134519 (2010).
  - <sup>38</sup> C.J. Olson Reichhardt, C. Reichhardt, and A.R. Bishop, Anisotropic sliding dynamics, peak effect, and metastability in stripe systems, *Phys. Rev. E* **83**, 041501 (2011).
  - <sup>39</sup> H.J. Zhao, V.R. Misko, and F.M. Peeters, Dynamics of self-organized driven particles with competing range interaction, *Phys. Rev. E* **88**, 022914 (2013).